Statistical Properties of Homogeneous and Isotropic Turbulence in He II Measured via Particle Tracking Velocimetry

Yuan Tang,[1,2] Shiran Bao,[1,2] Toshiaki Kanai,[1,3] and Wei Guo[1,2,*]

[1] *National High Magnetic Field Laboratory, 1800 East Paul Dirac Drive, Tallahassee, Florida 32310, USA*
[2] *Mechanical Engineering Department, Florida State University, Tallahassee, Florida 32310, USA*
[3] *Department of Physics, Florida State University, Tallahassee, Florida 32306, USA*

(Dated: July 1, 2020)

Despite being a quantum two-fluid system, superfluid helium-4 (He II) is observed to behave similarly to classical fluids when a flow is generated by mechanical forcing. This similarity has brought up the feasibility of utilizing He II for high Reynolds number classical turbulence research, considering the small kinematic viscosity of He II. However, it has been suggested that the non-classical dissipation mechanism in He II at small scales may alter its turbulent statistics and intermittency. In this work, we report our study of a nearly homogeneous and isotropic turbulence (HIT) generated by a towed grid in He II. We measure the velocity field using particle tracking velocimetry with solidified deuterium particles as the tracers. By correlating the velocities measured simultaneously on different particle trajectories or at different times along the same particle trajectory, we are able to conduct both Eulerian and Lagrangian flow analyses. Spatial velocity structure functions obtained through the Eulerian analysis show scaling behaviors in the inertial subrange similar to that for classical HIT but with enhanced intermittency. The Lagrangian analysis allows us to examine the flow statistics down to below the dissipation length scale. Interestingly, abnormal deviations from the classical scaling behaviors are observed in this regime. We discuss how these deviations may relate to the motion of quantized vortices in the superfluid component in He II.

I. INTRODUCTION

Below about 2.17 K, liquid ^{4}He undergoes a second-order phase transition to the superfluid phase (He II). Phenomenologically, He II can be described by Landau's two-fluid model [1]. This mesoscopic model treats the system as consisting of two fully miscible fluid components: an inviscid superfluid component (i.e., the condensate) and a viscous normal-fluid component (i.e., the thermal excitations) [2]. The rotational motion in the superfluid can occur only with the formation of topological defects in the form of quantized vortex lines [3]. These vortex lines all have identical cores (thickness $\xi_0 \simeq 1$ Å) and they each carry a single quantum of circulation $\kappa \simeq 10^{-3}$ cm^2/s. Turbulence in the superfluid takes the form of an irregular tangle of vortex lines (quantum turbulence) [4]. The normal fluid behaves more like a classical fluid. But a force of mutual friction between the two fluids [5], arising from the scattering of thermal excitations by the vortex lines, can affect the flows in both fluids.

Despite being a quantum two-fluid system, He II has been observed to exhibit flow characteristics similar to that in classical fluids when the flows are generated by mechanical forcing [6, 7]. This similarity has brought up the feasibility of utilizing the small kinematic viscosity of He II (i.e., about three orders of magnitudes smaller than that of ambient air [8]) to generate turbulent flows with extremely high Reynolds numbers for classical turbulence research and model testing [9, 10]. The quasiclassical behavior of He II in mechanically driven flows is believed to be the result of a strong coupling of the two fluids at large scales by mutual friction [11]. The turbulent eddies in the normal fluid are matched by eddies in the superfluid induced by local polarization of the vortex tangle [12]. However, at small scales, especially below the mean inter-vortex distance ℓ, this coupling must break down because the superfluid flow is then controlled by the circulation around individual vortex lines and cannot match the classical normal-fluid flow. Therefore, a mutual friction dissipation sets in at these small scales, in addition to the viscous dissipation in the normal fluid [4]. The extend of the coupling at large scales and the unique small-scale dissipation mechanism all depend on the density ratio of the two fluids (and hence the temperature), which can give rise to subtle differences between He II quasiclassical flows and flows in classical fluids. For instance, a past theoretical work suggested a temperature-dependent enhancement of turbulence intermittency in He II quasiclassical flows [13]. In order to explore these interesting similarities and differences, quantitative velocity-field measurements in a simple and well-controlled He II quasiclassical flow are needed.

A simple form of turbulence that has received extensive attention in classical fluids research is the so-called homogeneous isotropic turbulence (HIT) [14–16], which can also be achieved in He II in the wake of a towed grid [6]. In a

* Corresponding: wguo@magnet.fsu.edu

recent work, we reported the study of grid turbulence in a He II filled channel using a molecular tagging velocimetry (MTV) technique [17]. This technique is based on the creation and tracking of thin lines of He_2^* molecular tracers [18]. These tracers are completely entrained by the viscous normal fluid above 1 K and therefore their motion provides unambiguous information about the normal-fluid flow [19–25]. A striking nonmonotonic temperature-dependent intermittency enhancement was observed for the first time [17]. Nevertheless, there are two major limitations in the MTV experiment: 1) the MTV method only allows the measurement of the velocity component perpendicular to the tracer lines [26], and hence there lacks information about the isotropicity of the flow; and 2) the spatial resolution is limited by the displacement of the tracer lines (i.e., 100-200 μm), which is greater than the typical dissipation length scale (i.e., a few tens of microns).

To overcome these issues, we report in the present work the application of a particle tracking velocimetry (PTV) technique for velocity-field measurements in a recently built He II grid turbulence facility [27]. Micron-sized solidified deuterium particles are used as the tracers, whose motion can be tracked with a spatial resolution of a few microns to render both the horizontal and the vertical velocities within the imaging plane. These particles experience the drag force from the viscous normal fluid. As we will discuss later, the corresponding Stokes number is about 0.16 in our experiment, which means they do faithfully follow the normal fluid motion. These tracers have no appreciable interaction with the superfluid, but they can get trapped on the vortices due to the superfluid Bernoulli pressure [3]. This trapping may render their motion hard to interpret in He II flows where the two fluids have different mean velocities (e.g., heat-induced thermal counterflow [1]) [28–31]. However, this issue is not a concern in grid turbulence. At large scales where the two fluids are nearly coupled, the motion of the particles can provide us quantitative information about the coupled velocity field. At small scales, deviations from the classical turbulence statistics may be unveiled due to the motion of the trapped particles.

In Sec. II, we briefly describe the experimental setup and the measurement methods. In Sec. III, we first present evidences to show that a nearly HIT can emerge in the decay of the towed-grid generated turbulence in He II. Then, by correlating the velocities measured simultaneously on different particle trajectories or at different times along the same particle trajectory, we manage to conduct both Eulerian and Lagrangian velocity statistical analyses. We show that the spatial velocity structure functions obtained through the Eulerian analysis exhibit scaling behaviors in the inertial subrange similar to that for classical HIT but with enhanced intermittency. The Lagrangian analysis, on the other hand, allows us to examine the flow statistics down to below the dissipation length scale. In this regime, abnormal deviations from the classical scaling behaviors are observed. We discuss how these deviations may relate to the motion of the quantized vortices. A brief summary is provided in Sec. IV.

II. EXPERIMENTAL METHOD

The experimental apparatus used in the current work was designed and built specifically for PTV-based He II grid-turbulence research [27]. As shown schematically in Fig. 1, a transparent cast acrylic flow channel with a square cross section (D^2=1.6×1.6 cm^2, length: 33 cm) is immersed vertically in a He II bath, where the helium temperature can be controlled by regulating the vapor pressure in the bath. A brass mesh grid is suspended by four stainless-steel thin wires at the four corners inside the flow channel. These wires are connected to the drive shaft of a linear motor system. A LabVIEW computer program is developed to control the motor system such that the grid can be pulled at a constant speed between 0.1 and 60 cm/s. In this specific work, we use a fixed grid speed at 30 cm/s. In order to minimize possible large-scale secondary flows around the moving grid, we followed the guidelines from classical grid turbulence research [32, 33] and designed our grid to have a mesh spacing of 3 mm and an open area of 40% and with special treatments of its boundary and the four corners [27].

To probe the flow, solidified deuterium particles are used as the tracers. These particles are produced by slowly injecting a room-temperature mixture of 5% deuterium gas and 95% helium gas through a leak valve into the flow channel [34]. The gas mass flow rate is restricted such that the injection does not affect the bath temperature. Typically, the resulting particles have diameters in the range 3 to 6 μm with a mean $d_p \simeq 5$ μm, as determined from their settling velocity in quiescent He II [27]. A continuous-wave laser sheet (thickness: 200 μm, height: 9 mm) passes through the geometric center of the channel to illuminate the particles. We then pull the grid at the controlled speed and use a high-speed camera (120 frame per second) to record the motion of the particles. Due to the camera's limited internal memory, we record the particle motion for a period of 0.28 s (i.e., 34 frames) for every 2 s following the passage of the grid. Particle trajectories can be extracted from the sequence of images based on the feature-point tracking routine developed by Sbalzarini and Koumoutsakos [35].

Besides the PTV measurement, a standard second-sound attenuation method is also used to measure the temporal evolution of the spatial-averaged vortex-line density $L(t)$ (i.e., total length of the vortices per unit volume, $L^{-1/2} = \ell$) [27]. The turbulence generated by the towed grid decays with time. We take the instant when the grid passes through the center of the view port as the time origin for both the visualization and the second-sound measurements. These

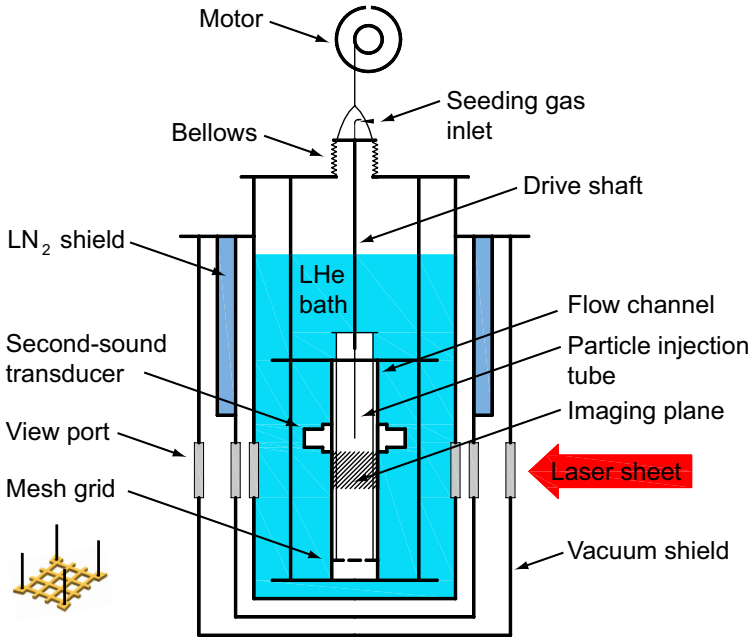

FIG. 1: Schematic diagram of the experimental apparatus.

measurements are made in the temperature range of 1.65 to 2.12 K. At each temperature, we normally repeat the experiment 10 times so that an ensemble statistical analysis of the particle trajectories can be performed at different decay times.

III. EXPERIMENTAL RESULTS AND DISCUSSIONS

A. Temporal evolution of the grid turbulence

It is generally believed that a moving grid in He II first produces turbulent eddies with sizes comparable to the mesh grid spacing. Then, after a short transient period, the energy-containing eddies saturate at sizes comparable to the width of the channel, which leads to a nearly HIT that decays with time [6]. However, the observation of large-scale flows right after the passage of the grid in our previous MTV experiment casts doubt on this simple physical picture [17]. These large-scale flows are likely due to the secondary flows caused by the imperfection of the grid geometry,

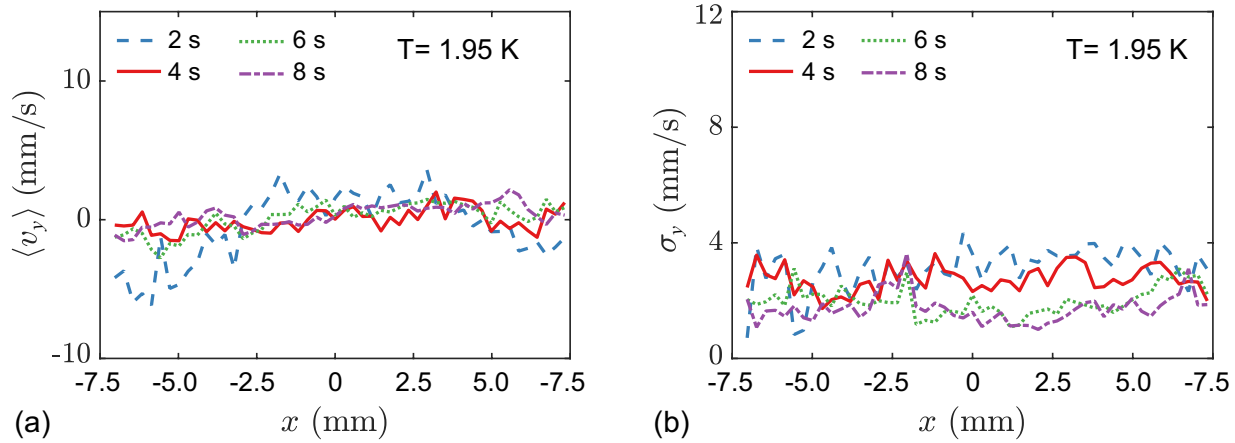

FIG. 2: (a) Ensemble-averaged vertical velocity $\langle v_y \rangle$ profile following the passage of the grid. (b) The corresponding vertical velocity variance σ_y. The data were taken at 1.95 K with a grid velocity of 30 cm/s.

which is hard to completely avoid. To examine the evolution of the velocity profile in our current experiment, we analyze the particle trajectories and calculate the vertical velocity v_y as a function of the horizontal position x across the width of the flow channel. Representative velocity profiles $\langle v_y(x)\rangle$ obtained at 1.95 K through an assemble average over many trajectories and over 10 experimental trials are shown in Fig. 2 (a). It is obvious that large-scale nonuniform flows exist at short decay times, despite the careful design of the grid. Nevertheless, these nonuniform flows have evolved to a more uniform turbulence by $t = 4$ s such that $\langle v_y(x)\rangle$ becomes nearly zero across the channel width. Fig. 2 (b) shows the profile of the corresponding vertical-velocity variance σ_y, defined as $\sigma_y = \left\langle [v_y(x) - \overline{v}_y]^2 \right\rangle^{1/2}$. It appears that σ_y is more spatially homogeneous and remains at a relatively high level at $t = 4$ s.

In Fig. 3, we show the calculated probability density functions (PDFs) of the particle horizontal velocity v_x and the vertical velocity v_y obtained at 1.95 K. At small decay times, the vertical velocity PDFs exhibit double-peak structures, which reflect the nonuniform large-scale eddies as revealed in Fig. 2 (a). After these large-scale eddies decay, the velocity PDFs can be fitted reasonably well by Gaussian functions. Through such fits, the evolution of the velocity variances in both the horizontal direction $\sigma_x(t)$ and the vertical direction $\sigma_y(t)$ can be obtained, which provides us information about the decay of the turbulence kinetic energy density $K_x(t) = \frac{1}{2}\sigma_x(t)^2$ and $K_y(t) = \frac{1}{2}\sigma_y(t)^2$.

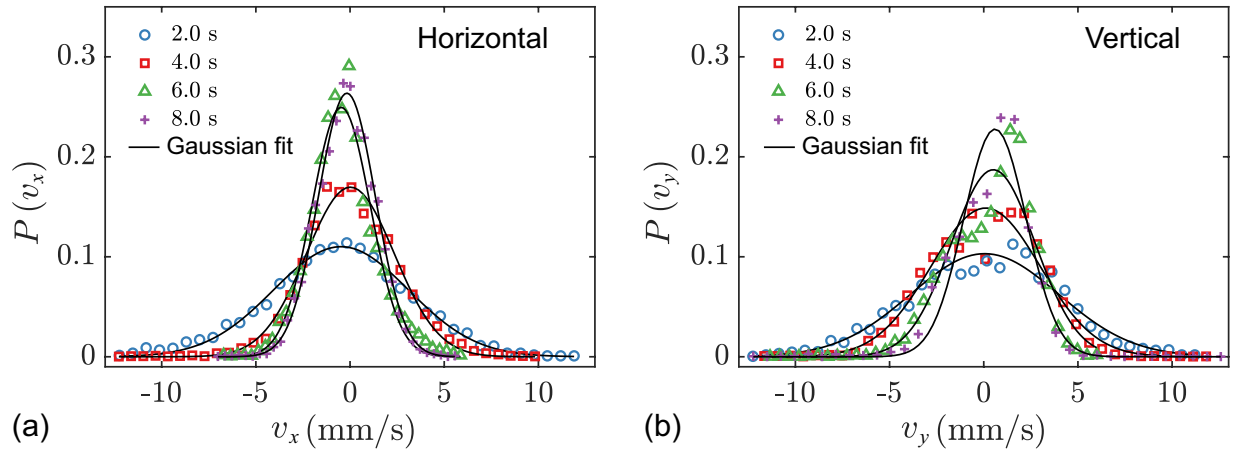

FIG. 3: Horizontal (a) and Vertical (b) particle velocity PDFs at different decay times as indicated. The data were taken at 1.95 K with a grid velocity of 30 cm/s.

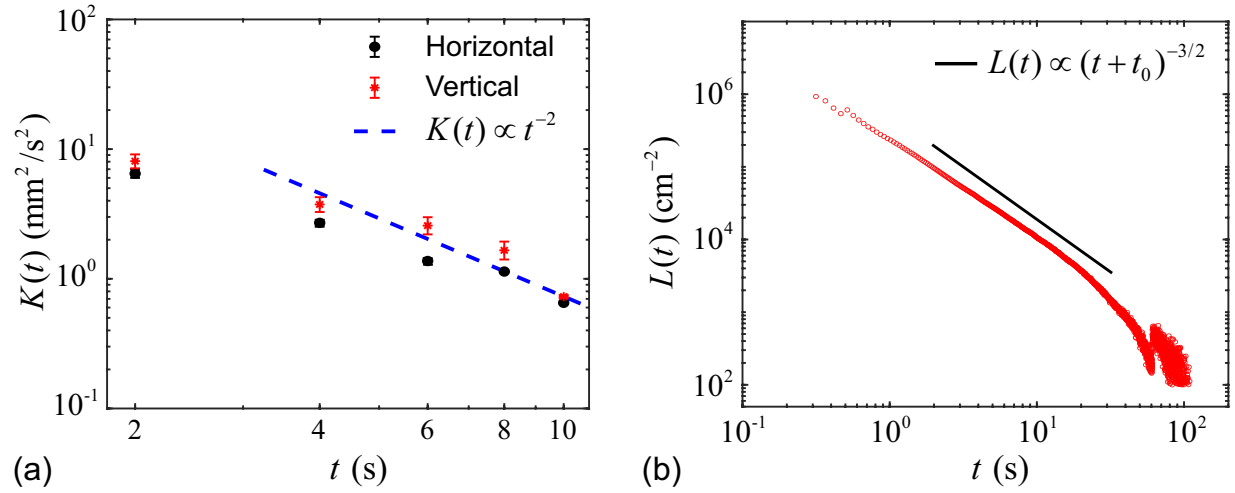

FIG. 4: (a) Time evolution of the turbulence kinetic energy $K(t)$ contribution from the horizontal and the vertical velocity components. (b) Decay of the quantized vortex-line density $L(t)$. The solid black curve represents the scaling $L(t) \propto (t + t_0)^{-3/2}$, where $t_0 = 0.27$ s is the virtual time origin [36]. The data were taken at 1.95 K.

In Fig. 4, we show the time-evolution of the obtained turbulence kinetic energy $K(t)$ together with the measured vortex-line density $L(t)$. It turns out that $K(t)$ decays more or less accordingly to $K(t) \propto t^{-2}$, especially for $t \geq 4$ s.

The contributions to $K(t)$ from the two velocity components appear to have similar magnitudes, which suggests that the turbulence is relatively isotropic. The decay of the vortex-line density exhibits a scaling behavior of $L(t) \propto t^{-3/2}$ after the first a few seconds. According to refs. [6, 11, 37], both these scalings are considered as the characteristics of decaying HIT in He II after the sizes of the energy-containing eddies are saturated by the channel width. Based on these analyses, the turbulence at 4 s decay time appears to be reasonably homogeneous and isotropic, and its turbulence kinetic energy density is relatively high such that an inertial subrange may exist. In what follows, we shall focus on the data set taken at $t = 4$ s for detailed statistical analysis.

To aid the discussion of the statistical analysis, we would like to provide information about the characteristic time and length scales of the turbulence. For this purpose, the energy dissipation rate ϵ=-$d(K_x + K_y + K_z)/dt$ needs to be evaluated. In principle, one may determine ϵ through Fig. 4 (a). However, due to the limited data points and their large scattering, only a rough order of magnitude estimation of $\epsilon \approx$10 mm^2/s^3 can be made. We therefore adopt the method introduced in ref. [38] to calculate ϵ based on velocity spatial derivatives. In this calculation, we select all the velocity pairs measured simultaneously at two particles that are separated by less than 0.1 mm to evaluate the ensemble averaged velocity spatial derivatives. ϵ=43.7 mm^2/s^3 is obtained for the data at 4 s decay time at 1.95 K. Using this value, we are able to calculate the Taylor microscale λ, Taylor Reynolds number Re_λ, Kolmogorov length scale η and time scale τ_η. The expressions of these parameters and their values are listed in Table I.

TABLE I: Characteristic parameters of the He II grid turbulence at 4 s decay time at 1.95 K.

Parameter	Expression [a]	Value
Energy dissipation rate ϵ (mm$^2/s^3$) [38]	$\epsilon = \nu\langle 4(\frac{\partial v_x}{\partial x})^2 + 4(\frac{\partial v_y}{\partial y})^2 + 3(\frac{\partial v_x}{\partial y})^2 + 3(\frac{\partial v_y}{\partial x})^2 + 4(\frac{\partial v_x}{\partial x}\frac{\partial v_y}{\partial y}) + 6(\frac{\partial v_y}{\partial y}\frac{\partial v_y}{\partial x})\rangle$	43.7
Taylor microscale λ (mm)	$\lambda \approx \sqrt{15\frac{\nu}{\epsilon}}\langle v\rangle_{\rm rms}$, $\langle v\rangle_{\rm rms} = \sqrt{[2(\sigma_x)^2 + (\sigma_y)^2]/3}$	0.14
Kolmogorov microscale η (μm)	$\eta = (\frac{\nu^3}{\epsilon})^{1/4}$	11.9
Taylor Reynolds number Re_λ	$Re_\lambda = \frac{\langle v\rangle_{\rm rms}\lambda}{\nu}$	34.5
Large scale Reynolds number Re_D	$Re_D = \frac{\langle v\rangle D}{\nu}$, $\langle v\rangle = \langle 2(v_x)^2 + (v_y)^2\rangle^{1/2}$	6.7×10^3
Kolmogorov time scale τ_η (ms)	$\tau_\eta = (\frac{\nu}{\epsilon})^{1/2}$	14.8
Stokes time τ_s (ms)	$\tau_s = \frac{\rho_p d_p^2}{18\mu}$	0.20

[a] ν and μ denote the kinematic viscosity and the dynamics viscosity of He II [8], respectively.

We have also calculated the Stokes time of the tracers τ_s and included it in Table I. The small Stokes time gives a Stokes number (i.e., St=$\tau_s\langle v\rangle/d_p$) of about 0.16, suggesting excellent tracing accuracy [39]. It is worthwhile noting that our sampling time (i.e., inverse of the camera frame rate) is 8.3 ms, which is smaller than the Kolmogorov time and greater than the Stokes time. This is desired for high fidelity PTV measurements.

B. Eulerian structure functions and intermittency

In the Eulerian description of fluid flow, spatial structure functions are known to be very useful tools for characterizing the statistical properties of the turbulence [40]. For fully developed HIT, the relevant forms of the structure functions are the n-th order longitudinal and transverse structure functions, defined as [41, 42]:

$$S_n^{\parallel}(r) = \langle|\delta\mathbf{V}(\mathbf{r})\cdot\hat{\mathbf{r}}|^n\rangle \quad \text{and} \quad S_n^{\perp}(r) = \langle|\delta\mathbf{V}(\mathbf{r})\times\hat{\mathbf{r}}|^n\rangle \tag{1}$$

where $\delta\mathbf{V}(\mathbf{r}) = \mathbf{V}(\mathbf{r_1}) - \mathbf{V}(\mathbf{r_2})$ denotes the difference of the velocities measured simultaneously at two locations that are separated by $\mathbf{r} = \mathbf{r_1} - \mathbf{r_2}$, and the angle brackets represent the ensemble average. For fully-developed ideal HIT in an incompressible fluid, these structure functions exhibit the well-known Kolmogorov-Obukhov scaling behaviors [43, 44]. Specifically, the third-order structure function should scale as $|S_3(r)| = \frac{4}{5}\epsilon r$. The range of r over which this scaling holds defines the inertial subrange of the turbulence energy cascade. In this inertial subrange, the second-order structure function is expected to scale as $S_2(r) \propto r^{2/3}$.

To check whether an inertial subrange develops in our grid turbulence, we have performed Eulerian analysis of the velocity field by correlating the velocities measured simultaneously on different particle trajectories (see Appendix A

for more details). The range of r in this analysis is set by our requirement that the sample number at a given particle separation r must be greater than 10^2. To our knowledge, no prior PTV experiments with He II have ever reported the implementation of the Eulerian analysis [45, 46]. In Fig. 5 (a1) and (a2), we show the calculated $S_3^{\parallel}(r)$ and $S_3^{\perp}(r)$ compensated by $(\epsilon r)^{-1}$ for the data set obtained at $t = 4$ s. Over the range 0.12 mm$\leq r \leq$2 mm as highlighted by the shaded region, both $S_3^{\parallel}(r)/\epsilon r$ and $S_3^{\perp}(r)/\epsilon r$ appear to be more or less flat and their values are indeed close to 4/5, indicating the existence of a cascade inertial subrange. The lower end of this subrange agrees well with the calculated Taylor microscale λ=0.14 mm. We also plot the second-order structure functions in Fig. 5 (b1) and (b2). It is clear that in the inertial subrange, both $S_2^{\parallel}(r)$ and $S_2^{\perp}(r)$ can be well fitted by power-law scalings that are close to $r^{2/3}$.

The Kolmogorov-Obukhov scalings of the higher-order structure functions in the inertial subrange in an ideal HIT are $S_n(r) \propto r^{\frac{n}{3}}$ [47]. However, intermittency can occur spontaneously in real turbulent flows, which manifests itself as extreme velocity excursions that appear more frequently than one would expect on the basis of Gaussian statistics. Corrections to the scaling exponents of the velocity structure functions are therefore expected, especially for higher-order structure functions that are more sensitive to the occurrence of rare events. She and Leveque proposed a universal scaling $S_n(r) \propto r^{\zeta_n}$ for HIT in classical fluids [48], where $\zeta_n = \frac{n}{9} + 2\left[1 - (\frac{2}{3})^{n/3}\right]$. These predicted scalings were confirmed experimentally by Benzi *et al.* [49]. To examine the scaling behaviors of the structure functions and the intermittency in He II grid turbulence, we adopt the extended self-similarity (ESS) method by plotting $S_n(r)$ versus $S_3(r)$ (instead of r) in the inertial subrange [49, 50]. It is known that the ESS analysis can reveal scaling laws even for turbulent flows with moderate Reynolds numbers [51], thereby allowing for more accurate determination of the scaling exponents [52]. In Fig. 6, we show the calculated $S_n^{\parallel}(r)$ and $S_n^{\perp}(r)$ versus $S_3(r)$. Clear power-law dependance of $S_n^{\parallel}(r)$ and $S_n^{\perp}(r)$ on $S_3(r)$ that extends beyond the inertial subrange is observed. We must emphasize that a reliable determination of the higher order statistics requires more samples. Unfortunately, our current data

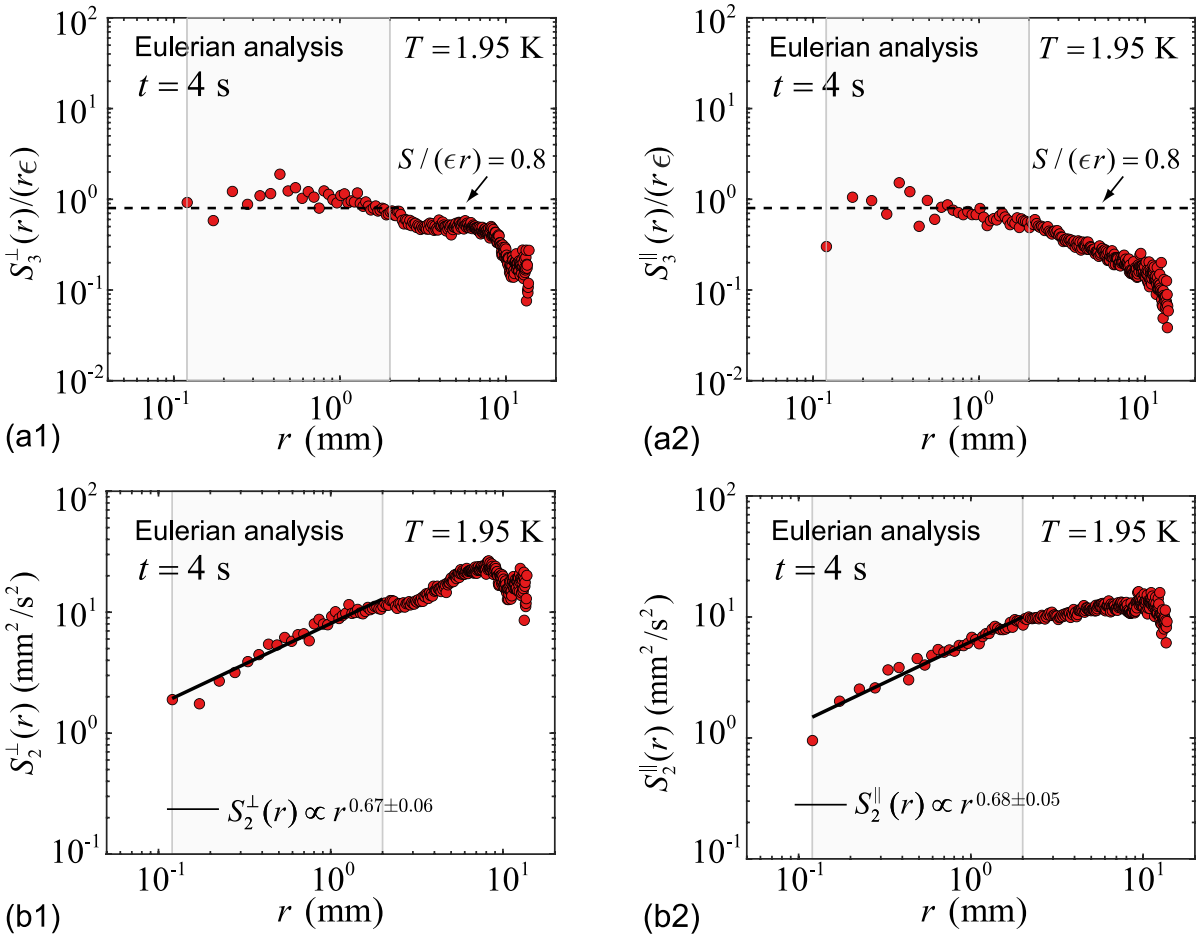

FIG. 5: (a1) and (a2) show the compensated third-order transverse and longitudinal structure functions. The dashed horizontal lines mark the constant value of 4/5. The shaded region indicates the inertial subrange. (b1) and (b2) show the second-order structure functions. The solid lines are power-law fits to the data in the shaded region.

sets are relatively limited due to various constrains such as the helium boil off, the long waiting time between runs, and the high cost of liquid helium for repeating the experiments.

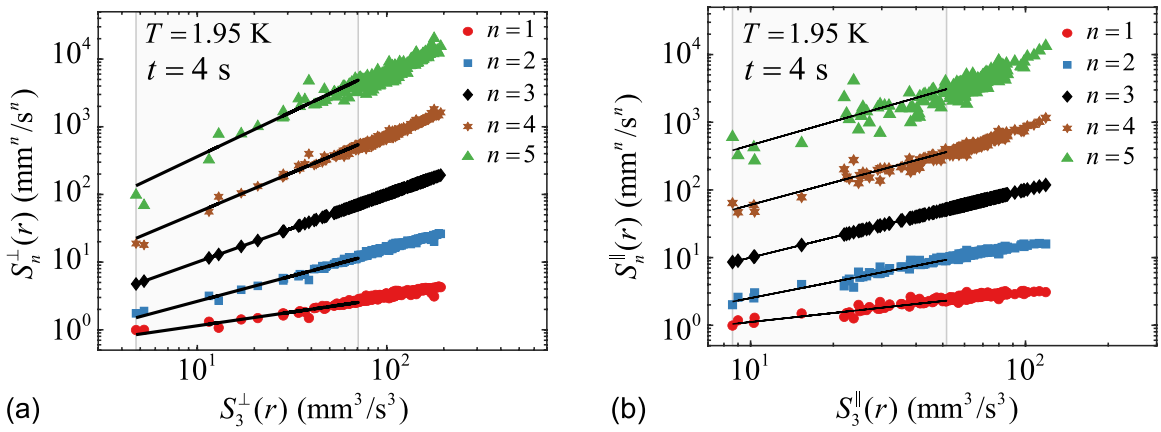

FIG. 6: Extended self-similarity plots of (a) transverse and (b) longitudinal velocity structure functions for $n = 1 \sim 5$ versus the third-order structure functions. The solid lines are power-law fits to the data in the inertial subrange.

In Fig. 7, we show the scaling exponents ζ_n extracted through the power-law fits in the ESS analysis. The large error bars are due to the relatively strong scattering of the data points in the fits. Besides the data obtained at 1.95 K (48.2% normal fluid), the results of similar measurements conducted at 1.65 K (19.3% normal fluid) and 2.12 K (78.8% normal fluid), together with the ζ_n values that She and Leveque proposed for classical fluids [48], are also collected in Fig. 7. The differences between ζ_n and the Kolmogorov-Obukhov scalings of $n/3$ are clearly seen in our data, which confirms the existence of intermittency in He II grid turbulence. The observation that ζ_n is universally smaller than $\frac{n}{3}$ for $n > 3$ agrees well with the ζ_n behavior in classical fluids [53]. Furthermore, it is clear that the intermittency in He II grid turbulence for $n > 3$ is enhanced compared to that in classical fluids, which agrees with theoretical predictions [13]. However, due to the large error bars associated with the extracted ζ_n, we cannot draw any definite conclusion regarding the temperature dependance of the intermittency in He II [17, 50, 54].

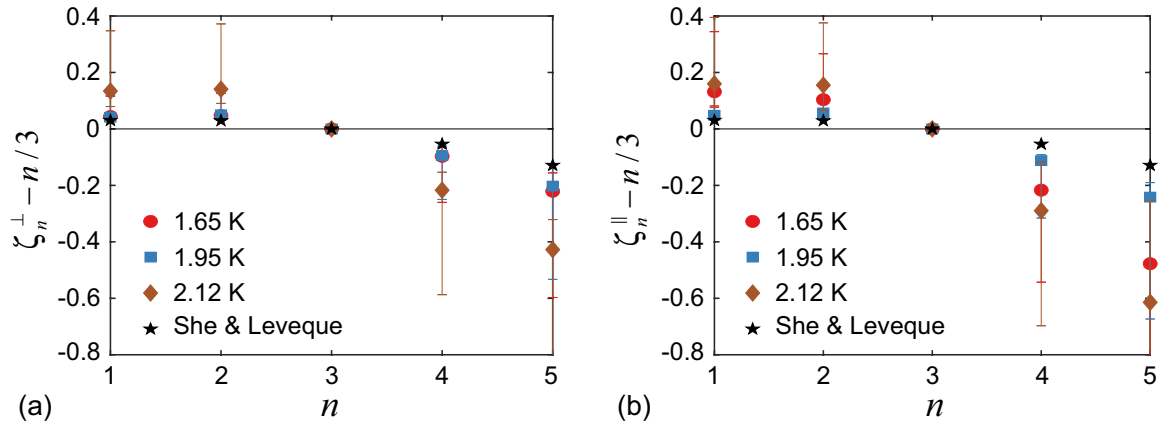

FIG. 7: Intermittency corrections to the scaling exponents of the transverse (a) and longitudinal (b) structure functions for He II grid turbulence. The corrections for classical fluids are also included for comparison [48].

C. Lagrangian analysis at small length scales

We have also conducted Lagrangian analysis of the particle motion by correlating the velocities measured along individual particle trajectories at different times. Conventionally, temporal structure functions in the Lagrangian framework can be constructed as:

$$S_n^{\parallel}(\tau) = \langle |\delta \mathbf{V}(\tau) \cdot \hat{\mathbf{r}}|^n \rangle \quad \text{and} \quad S_n^{\perp}(\tau) = \langle |\delta \mathbf{V}(\tau) \times \hat{\mathbf{r}}|^n \rangle \tag{2}$$

where $\delta\mathbf{V}(\tau) = \mathbf{V}(t+\tau) - \mathbf{V}(t)$ denotes the difference of the velocities measured at $t+\tau$ and t along a single particle trajectory, and $\mathbf{r}$ is the displacement of the particle over the time interval τ. In order to make more direct comparison with the Eulerian structure functions, in what follows, we will calculate the Lagrangian structure functions and plot them as a function of the distance r instead of τ. This treatment allows us to examine the flow statistics down to scales as small as the particle displacement in one frame time (i.e., 8.3 ms).

Fig. 8 shows the calculated second-order Lagrangian structure functions for the representative case of the He II grid turbulence at 1.95 K and at the decay time $t = 4$ s. The range of r covered in the Lagrangian analysis overlaps partly with that in the previous Eulerian analysis, while the lower bound of r now extends down to about 15 μm, which is much smaller than the mean inter-vortex distance ℓ (i.e., about 54 μm based on Fig. 4 (b)). Interestingly, in the overlapping region of r, the Lagrangian structure function data appear to agree quite well with that of the Eulerian analysis. This suggests that despite the different physical bases for the calculations of the Lagrangian and the Eulerian structure functions, they both exhibit similar scalings and magnitudes in the inertial subrange.

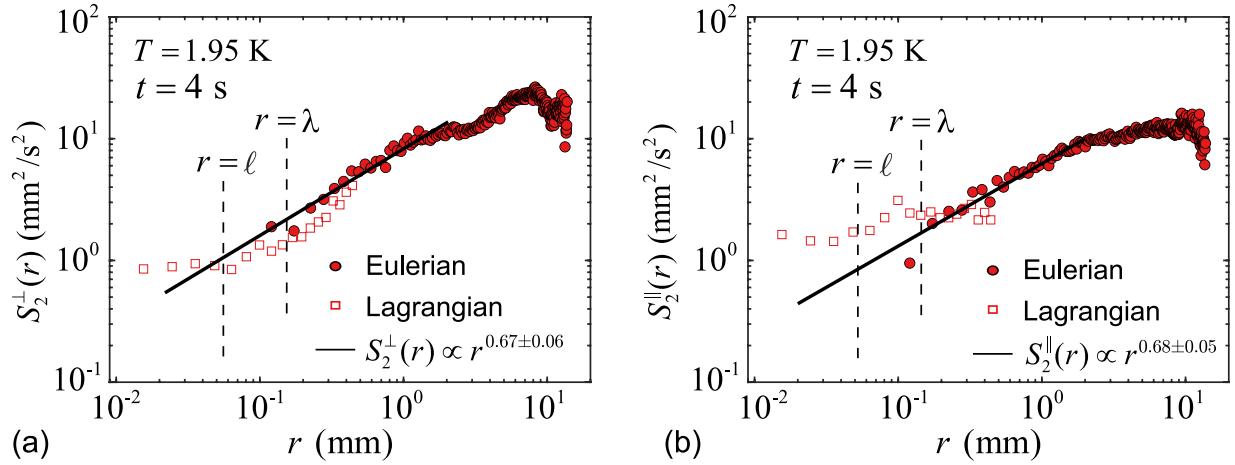

FIG. 8: Second-order (a) transverse and (b) longitudinal velocity structure functions obtained through both the Lagrangian and the Eulerian analyses of the particle trajectories for the data set obtained at 1.95 K and $t = 4$ s.

The more striking feature as revealed in Fig. 8 is the deviation of the Lagrangian structure functions from the inertial-subrange scaling at length scales below about 50 μm, i.e., comparable to the mean inter-vortex distance ℓ. Similar deviations are also observed at other temperatures. Indeed, the appearance of the deviation is not too surprising, because we know the energy dissipation must set in at length scales comparable to ℓ [24], which terminates the inertial energy cascade. However, in classical turbulence, it has been known that the viscous dissipation leads to an asymptotic scaling of the second-order structure function as $S_2(r) \propto r^2$ at small scales [47, 53]. This means that if the grid turbulence in He II truly behaves classically, one would see the $S_2(r)$ value drop rapidly in the dissipation subrange instead of rising above the inertial-subrange scaling curve. Therefore, an outstanding question is what causes the observed abnormal behavior of $S_2(r)$ at small scales.

To provide our thoughts on this question, let us consider what the tracer particles actually trace in He II grid turbulence. Note that these micron-sized particles can either get trapped on quantized vortices in the superfluid or entrained by the viscous normal fluid [31, 55, 56]. At length scales much greater than ℓ, the two fluids are coupled by the mutual friction. Therefore, regardless whether the particles are trapped or not, their motion at large scales simply provides information about the coupled velocity field. At small scales where the normal-fluid motion is strongly damped by viscosity and the mutual friction [24], the particles entrained by the normal fluid would make little contributions to the ensemble-averaging calculation of $S_2(r)$. On the other hand, for those trapped particles, their motions at small scales are controlled by the dynamics of individual quantized vortices. Even at scales below ℓ, the vortices still move randomly with a characteristic mean velocity $\langle v_L^2 \rangle^{1/2}$ given by [4, 24]:

$$\langle v_L^2 \rangle^{1/2} = \frac{\kappa}{4\pi} \left\langle \frac{1}{R^2} \ln^2 \left(\frac{R}{\xi_0} \right) \right\rangle^{1/2}, \tag{3}$$

where R is the local curvature radius of the vortices. Therefore, the trapped particles can lead to appreciable values of $S_2(r)$ at small scales. The exact behavior of $S_2(r)$ in the dissipation subrange will then depend on the fraction of the particles that are trapped and the temporal velocity correlations of the vortices. We would like to point out that moving vortices can generate wake structures in the normal fluid due to the mutual friction [31, 57, 58]. If an

untrapped particle moves through such wake structures, it may experience velocity variations which also lead to a finite contribution to $S_2(r)$ in the dissipation subrange. However, due to the small sizes of the wake structures, the dominant contribution to $S_2(r)$ should still come from the trapped particles. To test this physical picture, numerical simulations that can track the particles coupled to both the viscous normal fluid and the quantized vortices are needed [59, 60], which is beyond the scope of this work.

Finally, we perform the ESS analysis of the Lagrangian structure functions with $n = 1 \sim 5$ and plot them together with the Eulerian structure functions in Fig. 9. The Lagrangian structure functions extend to regions with smaller values of $S_3(r)$. Interestingly, despite the fact that the Lagrangian structure function data largely fall in the dissipation subrange, they appear to follow nicely the power-law scalings of the Eulerian data in the inertial subrange. This observation confirms the conclusion from classical turbulence research that the ESS scalings can encompass both the inertial and the dissipation subranges [49, 61]. But we must note that these scalings in the dissipation range are not real scalings since the power-law relation between $S_3(r)$ and r is lost.

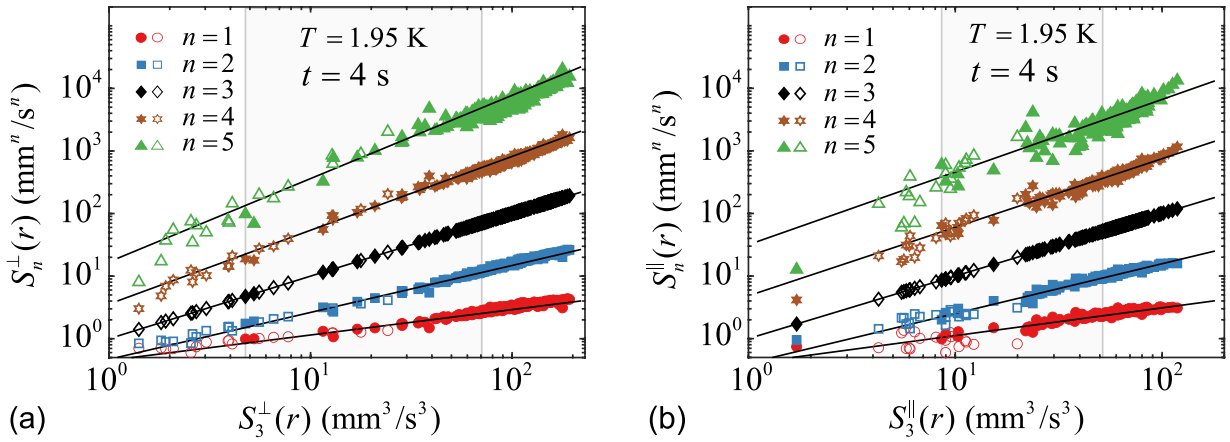

FIG. 9: Extended self-similarity plots of (a) transverse and (b) longitudinal structure functions based on both Lagrangian (empty symbols) and Eulerian (solid symbols) analyses of the particle trajectories for the data set obtained at 1.95 K and $t = 4$ s. The solid lines represent the power-law fits to the Eulerian data shown in Fig 6.

IV. SUMMARY

We have conducted PTV study of a nearly HIT in He II which emerges in the decay of the turbulent flow produced by a towed grid in a flow channel. By correlating the velocities measured simultaneously on different particle trajectories or at different times along the same particle trajectory, we have conducted both Eulerian and Lagrangian analyses of the turbulent velocity field. We find that the spatial velocity structure functions obtained through the Eulerian analysis exhibit scaling behaviors in the inertial subrange similar to that for classical HIT but the intermittency is obviously enhanced. The Lagrangian analysis allows us to obtain information about the velocity field in both the inertial subrange and the dissipation subrange. In the inertial subrange, the Lagrangian structure functions show similar magnitudes and scaling behaviors as the Eulerian counterparts. However, they deviate strongly from the classical scalings in the dissipation subrange. We propose that this abnormal behavior is related to the tracer particles which are trapped on quantized vortices, the verification of which requires numerical simulations that account for the coupling of the particles to both the normal fluid and the quantized vortices.

Appendix A: Sample number distribution in the Eulerian and Lagrangian analyses

As shown schematically in Fig. 10, the Eulerian velocity structure function analysis is conducted by correlating the velocities measured simultaneously on different particle trajectories. The range of r covered in this analysis is limited by the minimum and the maximum separation distances between the particle pairs. The Lagrangian structure function analysis is based on correlating the velocities measured along individual particle trajectories at different times. As discussed in the text, the Lagrangian structure functions are plotted as a function of the particle displacement r instead of the drift time τ. The corresponding range of r is then limited by the minimum and the maximum displacement of individual particles. In Fig. 11, we show the sample numbers extracted from a representative data

set (i.e., 10 trials with each having 34 frames lasting for 0.28 s) obtained at 1.95 K and at a decay time $t = 4$ s as a function of r. In order for improved accuracy in the ensemble-averaging calculations of the structure functions, we only analyze the data in the shaded region of r where the sample number is greater than 10^2.

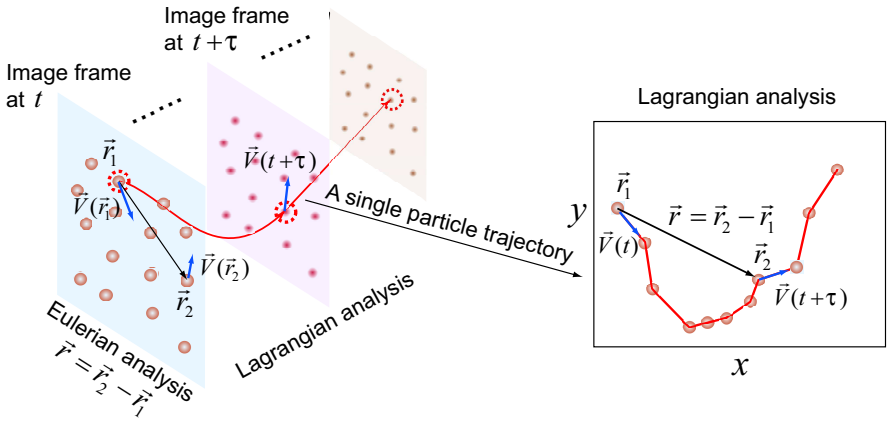

FIG. 10: Schematics showing the concept of the Eulerian and the Lagrangian velocity analyses.

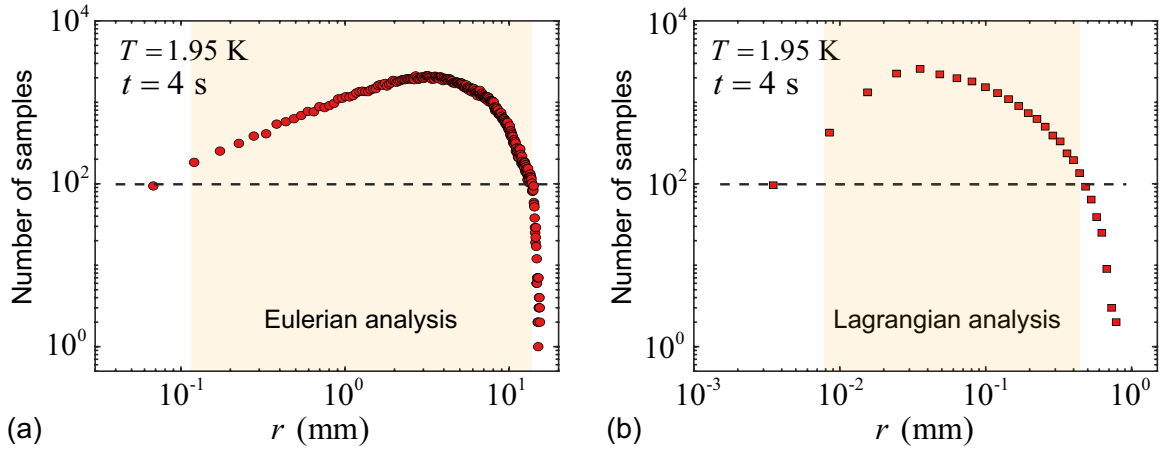

FIG. 11: Sample number as a function of r for (a) Eulerian and (b) Lagrangian velocity statistical analyses of the particle trajectories for the data set obtained at 1.95 K and $t = 4$ s. The analyses are conducted only in the shaded regions where the sample number is greater than 10^2.

ACKNOWLEDGMENTS

The authors would like to thank A. Pomyalov, W. F. Vinen, V. L'vov for valuable discussions. This work is supported by the National Science Foundation (NSF) under Grant No. DMR-1807291 and partially by U.S. Department of Energy under Grant No. DE-SC0020113. The experiment was conducted at the National High Magnetic Field Laboratory at Florida State University, which is supported through the NSF Cooperative Agreement No. DMR-1644779 and the state of Florida.

[1] L. Landau and E. Lifshitz, *Fluid mechanics*, 2nd ed. (Pergamon Press, Oxford, England, 1987).
[2] D. Tilley and J. Tilley, *Superfluidity and Superconductivity*, 3rd ed. (Institute of Physics, Bristol, 1990).
[3] R. J. Donnelly, *Quantized Vortices in Helium II* (Cambridge University Press, Cambridge, England, 1991).
[4] W. F. Vinen and J. J. Niemela, Quantum turbulence, J. Low Temp. Phys. **128**, 167 (2002).

[5] W. F. Vinen, Mutual friction in a heat current in liquid helium II. I. experiments on steady heat currents, Proc. Roy. Soc. A **240**, 114 (1957).
[6] S. R. Stalp, L. Skrbek, and R. J. Donnelly, Decay of grid turbulence in a finite channel, Phys. Rev. Lett. **82**, 4831 (1999).
[7] J. Maurer and P. Tabeling, Local investigation of superfluid turbulence, Europhys. Lett. **43**, 29 (1998).
[8] R. J. Donnelly and C. F. Barenghi, The observed properties of liquid helium at the saturated vapor pressure, J. Phys. Chem. Ref. Data **27**, 1217 (1998).
[9] K. R. Sreenivasan and R. J. Donnelly, Role of cryogenic helium in classical fluid dynamics: Basic research and model testing, Adv. Appl. Mech. **37**, 239 (2001).
[10] J. J. Niemela and K. R. Sreenivasan, The use of cryogenic helium for classical turbulence: Promises and hurdles, J. Low. Temp. Phys. **143**, 163 (2006).
[11] W. F. Vinen, Classical character of turbulence in a quantum liquid, Phys. Rev. B **61**, 1410 (2000).
[12] C. F. Barenghi, D. C. Samuels, G. H. Bauer, and R. J. Donnelly, Superfluid vortex lines in a model of turbulent flow, Phys. Fluids **9**, 2631 (1997).
[13] L. Boué, V. L'vov, A. Pomyalov, and I. Procaccia, Enhancement of intermittency in superfluid turbulence, Phys. Rev. Lett. **110**, 014502 (2013).
[14] G. Comte-Bellot and S. Corrsin, The use of a contraction to improve the isotropy of grid-generated turbulence, J. Fluid Mech. **25**, 657 (1966).
[15] H. Tennekes and J. L. Lumley, *A First Course in Turbulence* (The MIT Press, Boston, United States, 1972).
[16] M. Sinhuber, E. Bodenschatz, and G. P. Bewley, Decay of turbulence at high Reynolds numbers, Phys. Rev. Lett. **114**, 034501 (2015).
[17] E. Varga, J. Gao, W. Guo, and L. Skrbek, Intermittency enhancement in quantum turbulence in superfluid ^{4}He, Phys. Rev. Fluids **3**, 094601 (2018).
[18] J. Gao, A. Marakov, W. Guo, B. T. Pawlowski, S. W. Van Sciver, G. G. Ihas, D. N. McKinsey, and W. F. Vinen, Producing and imaging a thin line of He_2^* molecular tracers in helium-4, Rev. Sci. Instrum. **86**, 093904 (2015).
[19] A. Marakov, J. Gao, W. Guo, S. W. Van Sciver, G. G. Ihas, D. N. McKinsey, and W. F. Vinen, Visualization of the normal-fluid turbulence in counterflowing superfluid ^{4}He, Phys. Rev. B **91**, 094503 (2015).
[20] J. Gao, W. Guo, V. S. L'vov, A. Pomyalov, L. Skrbek, E. Varga, and W. F. Vinen, Decay of counterflow turbulence in superfluid ^{4}He, JETP Lett. **103**, 648 (2016).
[21] J. Gao, W. Guo, and W. F. Vinen, Determination of the effective kinematic viscosity for the decay of quasiclassical turbulence in superfluid ^{4}He, Phys. Rev. B **94**, 094502 (2016).
[22] J. Gao, E. Varga, W. Guo, and W. F. Vinen, Energy spectrum of thermal counterflow turbulence in superfluid helium-4, Phys. Rev. B **96**, 094511 (2017).
[23] J. Gao, E. Varga, W. Guo, and W. F. Vinen, Statistical measurement of counterflow turbulence in superfluid helium-4 using he_2 tracer-line tracking technique, J. Low Temp. Phys. **187**, 490 (2017).
[24] J. Gao, W. Guo, S. Yui, M. Tsubota, and W. F. Vinen, Dissipation in quantum turbulence in superfluid ^{4}He above 1 K, Phys. Rev. B **97**, 184518 (2018).
[25] S. Bao, W. Guo, V. S. L'vov, and A. Pomyalov, Statistics of turbulence and intermittency enhancement in superfluid ^{4}He counterflow, Phys. Rev. B **98**, 174509 (2018).
[26] W. Guo, Molecular tagging velocimetry in superfluid helium-4: Progress, issues, and future development, J. Low Temp. Phys. **196**, 60 (2019).
[27] B. Mastracci and W. Guo, An apparatus for generation and quantitative measurement of homogeneous isotropic turbulence in He II, Rev. Sci. Instrum. **89**, 015107 (2018).
[28] B. Mastracci, S. Takada, and W. Guo, Study of particle motion in He II counterflow across a wide heat flux range, J. Low Temp. Phys. **187**, 446 (2017).
[29] B. Mastracci and W. Guo, Exploration of thermal counterflow in He II using particle tracking velocimetry, Phys. Rev. Fluids **3**, 063304 (2018).
[30] B. Mastracci and W. Guo, Characterizing vortex tangle properties in steady-state He II counterflow using particle tracking velocimetry, Phys. Rev. Fluids **4**, 023301 (2019).
[31] B. Mastracci, S. Bao, W. Guo, and W. F. Vinen, Particle tracking velocimetry applied to thermal counterflow in superfluid ^{4}He: Motion of the normal fluid at small heat fluxes, Phys. Rev. Fluids **4**, 083305 (2019).
[32] H. Fernando and I. De Silva, Note on secondary flows in oscillating-grid, mixing-box experiments, Phys. Fluids. A-Fluid **5**, 1849 (1993).
[33] R. E. Honey, R. Hershberger, R. J. Donnelly, and D. Bolster, Oscillating-grid experiments in water and superfluid helium, Phys. Rev. E **89**, 053016 (2014).
[34] E. Fonda, K. R. Sreenivasan, and D. P. Lathrop, Sub-micron solid air tracers for quantum vortices and liquid helium flows, Rev. Sci. Instrum. **87**, 025106 (2016).
[35] I. F. Sbalzarini and P. Koumoutsakos, Feature point tracking and trajectory analysis for video imaging in cell biology, J. Struct. Biol. **151**, 182 (2005).
[36] L. Skrbek and S. R. Stalp, On the decay of homogeneous isotropic turbulence, Phys. Fluids **12**, 1997 (2000).
[37] L. Skrbek and K. R. Sreenivasan, Developed quantum turbulence and its decay, Phys. Fluids **24**, 011301 (2012).
[38] D. Xu and J. Chen, Accurate estimate of turbulent dissipation rate using PIV data, Exp. Therm. Fluid Sci. **44**, 662 (2013).
[39] C. Tropea, A. Yarin, and J. Foss, *Springer Handbook of Experimental Fluid Mechanics* (Springer, Berlin, Heidelberg, 2007).
[40] P. A. Davidson, *Turbulence: An Introduction for Scientists and Engineers* (Oxford University Press, Oxford, United Kingdom, 2004).

[41] G. Stolovitzky and K. R. Sreenivasan, Scaling of structure functions, Phys. Rev. E **48**, R33 (1993).
[42] R. Benzi, S. Ciliberto, C. Baudet, and G. R. Chavarria, On the scaling of three-dimensional homogeneous and isotropic turbulence, Physica D **80**, 385 (1995).
[43] A. N. Kolmogorov, The local structure of turbulence in incompressible viscous fluid for very large reynolds numbers, Dokl. Akad. Nauk SSSR **30**, 9 (1941).
[44] A. M. Obukhov, On the distribution of energy in the spectrum of turbulent flow, Dokl. Akad. Nauk SSSR **32**, 19 (1941).
[45] M. La Mantia, D. Duda, M. Rotter, and L. Skrbek, Lagrangian accelerations of particles in superfluid turbulence, J. Fluid Mech. **717**, R9 (2013).
[46] W. Kubo and Y. Tsuji, Lagrangian trajectory of small particles in superfluid he ii, J. Low Temp. Phys. **187**, 611 (2017).
[47] J. Hinze, *Turbulence*, 2nd ed. (MacGraw Hill, New-York, 1975).
[48] Z.-S. She and E. Leveque, Universal scaling laws in fully developed turbulence, Phys. Rev. Lett. **72**, 336 (1994).
[49] R. Benzi, S. Ciliberto, R. Tripiccione, C. Baudet, F. Massaioli, and S. Succi, Extended self-similarity in turbulent flows, Phys. Rev. E **48**, R29 (1993).
[50] J. Salort, B. Chabaud, E. Lévêque, and P.-E. Roche, Investigation of intermittency in superfluid turbulence, in *J. Phys.: Conf. Ser.*, Vol. 318 (IOP Publishing, 2011) p. 042014.
[51] R. Benzi, S. Ciliberto, C. Baudet, G. R. Chavarria, and R. Tripiccione, Extended self-similarity in the dissipation range of fully developed turbulence, Europhys. Lett. **24**, 275 (1993).
[52] B. Dubrulle, Intermittency in fully developed turbulence: Log-poisson statistics and generalized scale covariance, Phys. Rev. Lett. **73**, 959 (1994).
[53] G. Stolovitzky, K. R. Sreenivasan, and A. Juneja, Scaling functions and scaling exponents in turbulence, Phys. Rev. E **48**, R3217 (1993).
[54] E. Rusaouen, B. Chabaud, J. Salort, and P.-E. Roche, Intermittency of quantum turbulence with superfluid fractions from 0% to 96%, Phys. Fluids **29**, 105108 (2017).
[55] G. P. Bewley, D. P. Lathrop, and K. R. Sreenivasan, Superfluid helium: Visualization of quantized vortices, Nature **441**, 588 (2006).
[56] T. Zhang and S. W. Van Sciver, Large-scale turbulent flow around a cylinder in counterflow superfluid ^{4}He (He II), Nature Phys. **1**, 36 (2005).
[57] O. C. Idowu, A. Willis, C. F. Barenghi, and D. C. Samuels, Local normal-fluid helium II flow due to mutual friction interaction with the superfluid, Phys. Rev. B **62**, 3409 (2000).
[58] S. Yui, H. Kobayashi, M. Tsubota, and W. Guo, Fully coupled dynamics of the two fluids in superfluid ^{4}He: Anomalous anisotropic velocity fluctuations in counterflow, Phys. Rev. Lett. **124**, 155301 (2020).
[59] D. Kivotides, C. F. Barenghi, and Y. A. Sergeev, Interactions between particles and quantized vortices in superfluid helium, Phys. Rev. B **77**, 014527 (2008).
[60] D. Kivotides, Motion of a spherical solid particle in thermal counterflow turbulence, Phys. Rev. B **77**, 174508 (2008).
[61] A. Arneodo, C. Baudet, F. Belin, R. Benzi, B. Castaing, B. Chabaud, R. Chavarria, S. Ciliberto, R. Camussi, F. Chilla, *et al.*, Structure functions in turbulence, in various flow configurations, at Reynolds number between 30 and 5000, using extended self-similarity, Europhys. Lett. **34**, 411 (1996).